DNA-Mediated Exciton Coupling and Electron Transfer between Donor and Acceptor Stilbenes Separated by a Variable Number of Base Pairs

ARTICLE *in* JOURNAL OF THE AMERICAN CHEMICAL SOCIETY · AUGUST 2004

Impact Factor: 12.11 · DOI: 10.1021/ja048664m · Source: PubMed

6 AUTHORS, INCLUDING:

Frederick D Lewis
Northwestern University
320 PUBLICATIONS **9,152** CITATIONS
SEE PROFILE

Ligang Zhang
Chinese Academy of Sciences
25 PUBLICATIONS **444** CITATIONS
SEE PROFILE

Xiaobing Zuo
Argonne National Laboratory
96 PUBLICATIONS **2,052** CITATIONS
SEE PROFILE

Ryan Hayes
Andrews University
18 PUBLICATIONS **1,536** CITATIONS
SEE PROFILE

J|A|C|S
ARTICLES
Published on Web 06/11/2004

DNA-Mediated Exciton Coupling and Electron Transfer between Donor and Acceptor Stilbenes Separated by a Variable Number of Base Pairs

Frederick D. Lewis,*,† Yansheng Wu,§ Ligang Zhang,† Xiaobing Zuo,‡ Ryan T. Hayes,† and Michael R. Wasielewski*,†

Contribution from the Department of Chemistry, Northwestern University, Evanston, Illinois 60208-3113, and Chemistry Division, Argonne National Laboratory, Argonne, Illinois 60439

Received March 8, 2004; E-mail: lewis@chem.northwestern.edu; wasielew@chem.northwestern.edu

Abstract: The synthesis, steady-state spectroscopy, and transient absorption spectroscopy of DNA conjugates possessing both stilbene electron donor and electron acceptor chromophores are described. These conjugates are proposed to form nicked DNA dumbbell structures in which a stilbenedicarboxamide acceptor and stilbenediether donor are separated by variable numbers of A−T or G−C base pairs. The nick is located either adjacent to one of the chromophores or between two of the bases. Thermal dissociation profiles indicate that stable structures are formed possessing as few as two A−T base pairs. Circular dichroism (CD) spectra in the base pair region are characteristic of B-DNA duplex structures, whereas CD spectra at longer wavelengths display two bands attributed to exciton coupling between the two stilbenes. The sign and intensity of these bands are dependent upon both the distance between the chromophores and the dihedral angle between their transition dipoles [$\Delta\epsilon \approx R_{da}^{-2} \sin(2\theta)$]. Pulsed laser excitation of the stilbenediamide results in creation of the acceptor−donor radical ion pair, which decays via charge recombination. The dynamics of charge separation and charge recombination display an exponential distance dependence, similar to that observed previously for systems in which guanine serves as the electron donor. Unlike exciton coupling between the stilbenes, there is no apparent dependence of the charge-transfer rates upon the dihedral angle between donor and acceptor stilbenes. The introduction of a single G−C base pair between the donor and acceptor results in a change in the mechanism for charge separation from single step superexchange to hole hopping.

Introduction

The distance-dependent dynamics of photoinduced electron transfer in DNA has been investigated in several systems employing a probe molecule as the electron acceptor and the nucleobase guanine as the electron donor.[1,2] Guanine has a lower oxidation potential than adenine and the pyrimidine nucleobases, making possible the selective oxidation of guanine by excited acceptors which do not also oxidize adenine. We have employed hairpin-forming bis(oligonucleotide) conjugates possessing a stilbene-4,4′-dicarboxamide **Sa** linker (Chart 1) and a single G−C base pair separated from the linker by a variable number of A−T base pairs to study the dynamics of DNA-mediated charge separation and charge recombination.[1,3] Modification of the hairpin structure by addition of secondary electron donors has made it possible to investigate the dynamics of reversible hole transport between primary and secondary donors separated by one or two A−T base pairs.[4]

Both in our studies and other investigations of photoinduced charge transfer in DNA, the acceptor excited state and its anion radical are observed by transient absorption spectroscopy. However, the formation of the guanine cation radical can only be inferred, since its transient absorption is much weaker than that of the stilbene singlet and anion radical.[5] Thus we sought a system in which donor and acceptor probes are positioned at opposite ends of a duplex region of variable length and base pair composition. Barton and co-workers have employed tethered intercalator donor−acceptor systems to investigate electron transfer across intervening base pairs by means of fluorescence quenching.[6] However, they have not reported the distance dependence of charge separation and recombination dynamics

† Northwestern University.
‡ Argonne National Laboratory.
§ Present address: Bayer Diagnostics, East Walpole, MA.

(1) Lewis, F. D.; Wu, T.; Zhang, Y.; Letsinger, R. L.; Greenfield, S. R.; Wasielewski, M. R. *Science* **1997**, *277*, 673−676.
(2) (a) Fukui, K.; Tanaka, K.; Fujitsuka, M.; Watanabe, A.; Ito, O. *J. Photochem. Photobiol., B* **1999**, *50*, 18−27. (b) Wan, C.; Fiebig, T.; Schiemann, O.; Barton, J. K.; Zewail, A. H. *Proc. Natl. Acad. Sci. U.S.A.* **2000**, *97*, 14052−14055. (c) Hess, S.; Götz, M.; Davis, W. B.; Michel-Beyerle, M. E. *J. Am. Chem. Soc.* **2001**, *123*, 10046−10055. (d) Lewis, F. D.; Wu, Y. *J. Photochem. Photobiol., C* **2001**, *2*, 1−16.
(3) Lewis, F. D.; Wu, T.; Liu, X.; Letsinger, R. L.; Greenfield, S. R.; Miller, S. E.; Wasielewski, M. R. *J. Am. Chem. Soc.* **2000**, *122*, 2889−2902.
(4) Lewis, F. D.; Liu, J.; Zuo, X.; Hayes, R. T.; Wasielewski, M. R. *J. Am. Chem. Soc.* **2003**, *125*, 4850−4861.
(5) Shafirovich, V. Y.; Dourandin, A.; Huang, W.; Luneva, N. P.; Geacintov, N. E. *Phys. Chem. Chem. Phys.* **2000**, *2*, 4399−4408.
(6) Murphy, C. J.; Arkin, M. R.; Jenkins, Y.; Ghatlia, N. D.; Bossmann, S. H.; Turro, N. J.; Barton, J. K. *Science* **1993**, *262*, 1025−1029.

10.1021/ja048664m CCC: $27.50

Chart 1

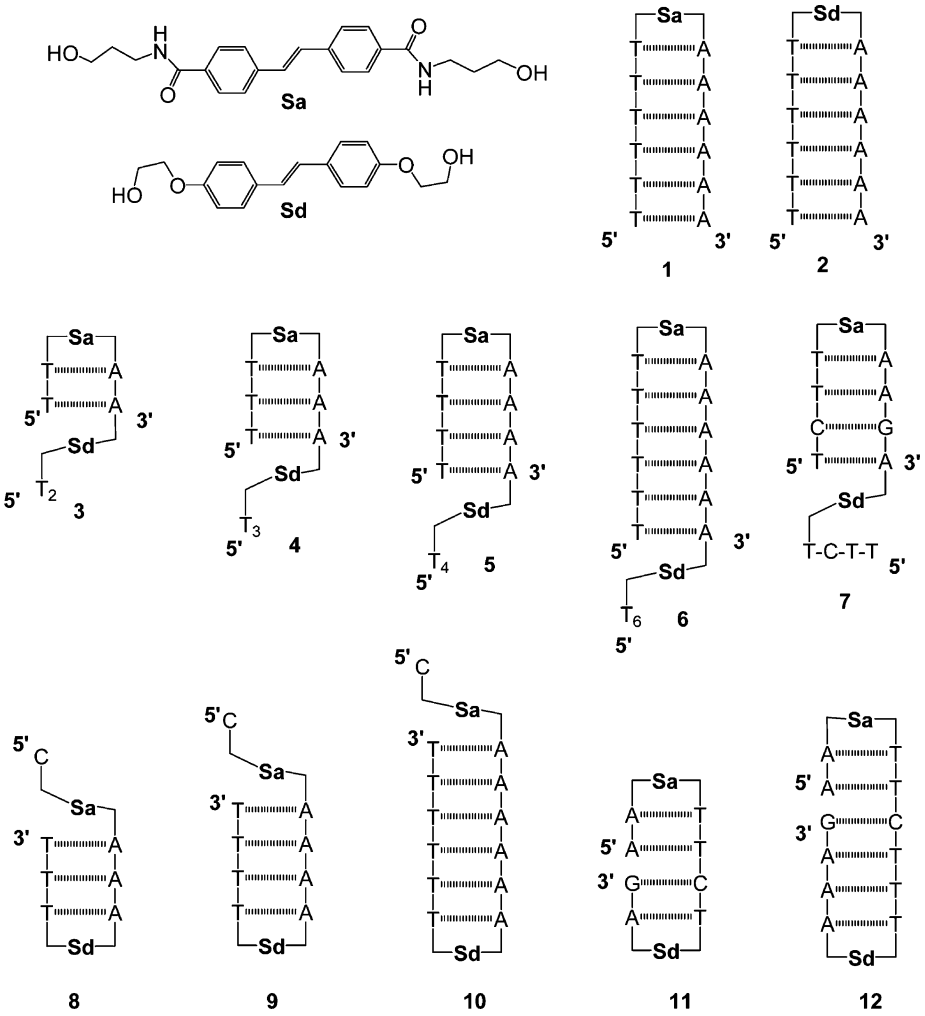

or the formation of both oxidized donor and reduced acceptor in such systems.

We report here an investigation of the circular dichroism (CD) spectra and photoinduced electron-transfer dynamics in modified hairpin conjugates possessing an **Sa** electron acceptor and stilbenediether **Sd** donor positioned at opposite ends of short duplex sequences (Chart 1, **3**−**12**).[7,8] The CD spectra of these conjugates display characteristic B-DNA bands at wavelengths shorter than 300 nm and longer wavelength bands attributed to exciton coupling between the two stilbenes, the amplitude and sign of which are dependent upon the number of base pairs separating the stilbenes. Analysis of the CD data supports the assignment of end-capped hairpin structures for conjugates **3**−**10** (rather than the triplex structures previously proposed for **3**−**7**[8]) and side-nicked dumbbell structures for conjugates **11** and **12** (Chart 1). Selective excitation of the **Sa** acceptor followed by charge separation yields the $\mathbf{Sa}^{-\bullet}-\mathbf{Sd}^{+\bullet}$ radical ion pair, which is directly observed by transient absorption spectroscopy. The dependence of the rate constants for charge separation and charge recombination upon the number of intervening base pairs is similar to that observed for systems with an **Sa** acceptor and guanine donor.[3] In addition, we observed the formation of long-lived charge-separated states in systems possessing a single G−C base pair located between the **Sa** acceptor and **Sd** donor as a consequence of hole transport via the G−C base pair. Comparison of the effect of **Sa**−**Sd** distance and orientation upon exciton coupling and charge separation reveals, for the first time, inherent differences between these two processes.

Results

Preparation of Conjugates. The preparation of *trans*-*N*,*N*′-bis(3-hydroxylpropyl)stilbene-4,4′-dicarboxamide (**Sa**) and *trans*-bis(2-hydroxylethyl)stilbene-4,4′diether (**Sd**) and conversion to their monoprotected, mono-activated diols by sequential reaction with 4,4′-dimethoxytrityl chloride and with 2-cyanoethyl diisopropylchlorophosphoramidite have been described.[9,10] The conjugates shown in Chart 1 were prepared by conventional phosphoramidite chemistry using a DNA synthesizer, as previously described for conjugates **1** and **2**. The 3′−3′ linkages between the Watson−Crick T:A hairpin sequence and the polyT strand attached to the **Sd** linker in conjugates **3**−**7** were accomplished by 5′ solid-phase oligonucleotide synthesis. Following synthesis, the conjugates were first isolated as trityl-on derivatives by RP-HPLC, then detritylated in 80% acetic acid for 30 min, and repurified by RP-HPLC as needed. The

(7) For a preliminary report of a portion of this research, see ref 8.
(8) Lewis, F. D.; Wu, Y.; Hayes, R. T.; Wasielewski, M. R. *Angew. Chem., Int. Ed.* **2002**, *41*, 3485−3487.
(9) Letsinger, R. L.; Wu, T. *J. Am. Chem. Soc.* **1995**, *117*, 7323−7328.
(10) Lewis, F. D.; Wu, Y.; Liu, X. *J. Am. Chem. Soc.* **2002**, *124*, 12165−12173.

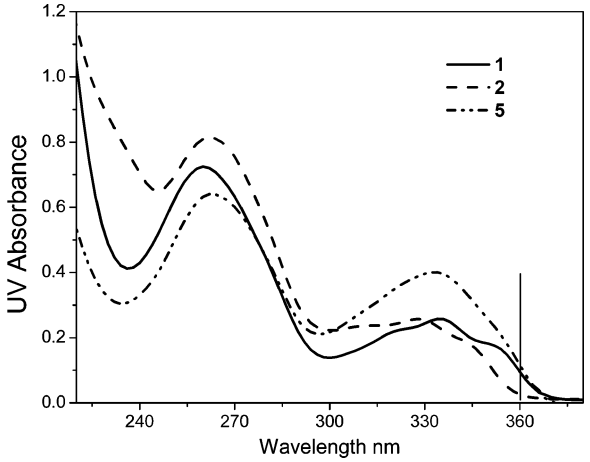

Figure 1. UV absorption spectra of the **Sa**- and **Sd**-linked conjugates **1**, **2**, and **5** in 10 mM sodium phosphate, pH 7.2, containing 0.1 M NaCl. Irradiation of **5** at 360 nm is absorbed primarily by **Sa**.

purified conjugates appeared as a single peak by both RP- and IE-HPLC and were characterized by UV, fluorescence, and CD spectroscopy. Molecular weights of representative purified conjugates were determined by ES−MS.

The 600 MHz 2D NMR spectrum of conjugate **6** was studied in an effort to obtain evidence for the formation of a triplex structure between the Watson−Crick duplex and the T_6 sequence attached to the **Sd** linker. The imino protons of the 5′-T_6 sequence attached to the **Sa** linker were readily assigned; however, the imino protons of the **Sd**−T_6 sequence could not be observed.

UV Spectra and Thermal Dissociation. The UV absorption spectra of conjugates **1**, **2**, and **5** are shown in Figure 1. Conjugates **1**−**12** display an absorption band near 260 nm, attributed to the overlapping absorption of the nucleobases and stilbene linkers, and a second band near 330 nm, attributed to the stilbene linkers. As previously reported, the **Sa**-linked conjugate **1** absorbs at slightly longer wavelength than the **Sd**-linked conjugate **2**.[3,10] The long-wavelength band of **5** is broader than those of **1** and **2**, as expected for a molecule possessing both **Sa** and **Sd** linkers. All of the donor−acceptor conjugates have absorption spectra similar to that of **5**.

The thermal dissociation profile for conjugates **3**−**6** determined at 260 nm in aqueous buffer containing 0.1 M NaCl is shown in Figure 2a. Cooling curves display only slight hysteresis. In each profile, there is a single melting transition at temperatures above 60 °C. At temperatures between 10 and 50 °C, there is a continuous increase in absorbance which becomes more pronounced as the total number of bases increases. Thermal dissociation profiles for **8**−**10** display a single transition at temperatures above 74 °C with little increase in absorbance below 50 °C. Profiles for **11**−**12** display a single melting transition which is considerably broader than those for **8**−**10**. The melting profiles of **10** and **12** are shown in Figure 2b, and values of T_M for **1**−**12** are summarized in Table 1.

Fluorescence Spectra. As previously reported, conjugate **1** is strongly fluorescent.[3] Its fluorescence quantum yield is 0.38 and decay time is 2.0 ns. In contrast, conjugate **2** is very weakly fluorescent ($\Phi_{fl} < 10^{-4}$), preventing determination of its singlet lifetime from fluorescence decay measurements.[11] Conjugates **3**−**12** are all fluorescent with band maxima and band shapes similar to that of **1**. The fluorescence intensity of these conjugates is highest when excited in the red-edge of the absorption

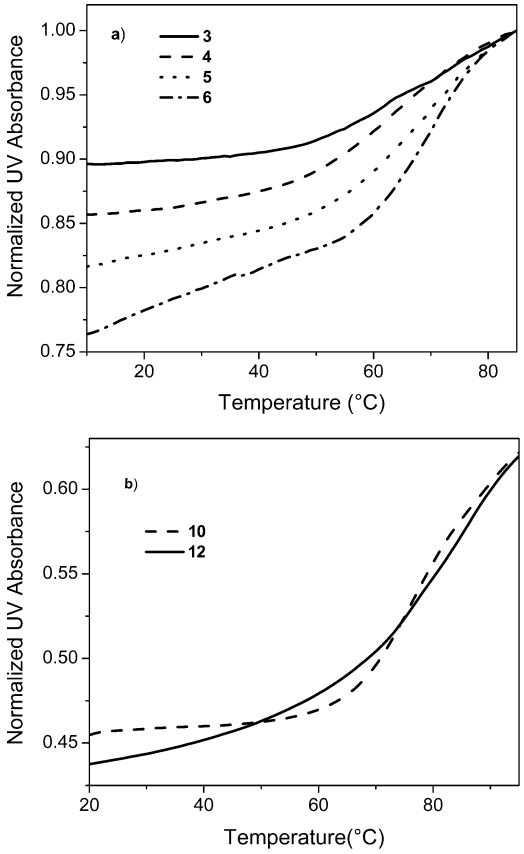

Figure 2. Thermal dissociation profiles for (a) conjugates **3**−**6** and (b) **10** and **12** in 10 mM sodium phosphate, pH 7.2, containing 0.1 M NaCl.

Table 1. Melting Temperatures for Conjugates **1**−**12**[a]

conjugate	T_M, °C	conjugate	T_M, °C
1	59	**7**	69
2	64	**8**	74
3	∼60	**9**	76
4	64	**10**	82
5	69	**11**	57
6	71	**12**	74

[a] Data for solutions containing 0.1 M NaCl and 10 mM phosphate buffer.

spectrum, where **Sa** absorbs more strongly than **Sd**. The fluorescence spectra of **3**−**6** obtained using 340 nm excitation are shown in Figure 3. The fluorescence intensity is seen to increase as the number of base pairs between the **Sa** and **Se** linkers is increased. Fluorescence quantum yields for **3**−**7** and **11**−**12** are summarized in Table 2. The values for all of these conjugates are smaller than those for **1**, indicative of the occurrence of variable degrees of fluorescence quenching. The fluorescence decay times for **5** and **6** are 1.2 ns and 1.4 ns, respectively. All of the other conjugates have fluorescence decay times shorter than the time-resolution of our instrumentation (ca. 0.5 ns).

Circular Dichroism Spectra. The CD spectra of poly(T)−poly(A) and conjugates **1** and **2** are shown in Figure 4a. At wavelengths shorter than 300 nm, the three spectra are similar, aside from the more pronounced 265 nm maximum for poly(T)−poly(A). Both **1** and **2** also display a weak, structureless band at wavelengths longer than 300 nm which is absent in the spectrum of poly(T)−poly(A). The CD spectra of **3**−**6** and

(11) Lewis, F. D.; Liu, X.; Miller, S. E.; Hayes, R. T.; Wasielewski, M. R. *J. Am. Chem. Soc.* **2002**, *124*, 11280−11281.

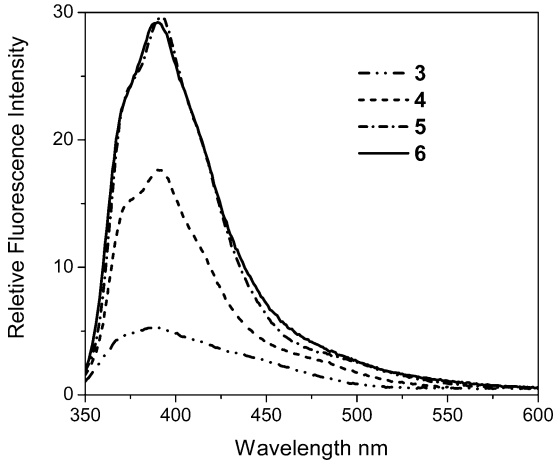

Figure 3. Fluorescence spectra of conjugates **3**−**6** in 0.1 M NaCl, 10 mM phosphate, pH 7.2 buffer, containing 0.1 M NaCl (λ_{ex} = 340 nm).

Table 2. Fluorescence Quantum Yields (Φ_{fl}) and Transient Decay Times (τ_S) for the **Sa** Singlet State, Transient Decay Times for the Ion Pair State (τ_I), and Rate Constants for Charge Separation (k_{cs}) and Charge Recombination (k_{cr})[a]

conjugate	Φ_{fl}[b]	τ_s,[c] ps	10^{-9} k_{cs},[d] s^{-1}	τ_I,[e,f] ns	10^{-7} k_{cr},[g] s^{-1}
1	0.38	2,000	<0.5		
2	$<10^{-3}$	<1		0.032	
3	0.06	75 (30)	13	8.4 (70)	12
4	0.18	280 (49)	3.1	130 (51)	0.77
5	0.32	540 (55)	1.3	5800 (45)	0.017
6	0.31	1800 (100)	0.05	*h*	
7	0.08	140 (37)	6.6	800 (25)	0.12
				6700 (38)	0.015
8		300 (54)	2.8	140 (64)	0.74
9		680 (64)	1.0	6,200 (36)	0.016
10		2000	0	*h*	
11	0.12	150 (45)	6.2	5600 (55)	0.017
12	0.14	130 (33)	7.2	5.9 (67)	17

[a] Data for ca. 10^{-6} M solutions in standard buffer (0.1 M NaCl, 10 mM sodium phosphate, pH 7.2). [b] Fluorescence quantum yields determined by comparison to quinine sulfate. Limits of error for multiple detection ±10%. [c] Transient decay at 575 nm assigned to the **Sa** singlet state, amplitude in parentheses. [d] Rate constant for charge separation, $k_{cs} = \tau_s^{-1} - \tau_1^{-1}$. [e] Decay component assigned to charge recombination of $\mathbf{Sa}^{-\bullet}$ determined at 575 nm, amplitude in parentheses. [f] Decay components determined at 525 nm and assigned to charge recombination of $\mathbf{Sd}^{+\bullet}$ are 8.2 ns for **3**, 145 ns for **4**, 8200 ns for **5**, and 5900 ns for **11**. [g] Rate constant for charge recombination, $k_{cr} = \tau_I^{-1}$. Average of 575 and 525 nm values where available. [h] No long-lived transient resolved.

8−**10** are shown in Figures 4b and 4c, respectively. At wavelengths below 300 nm, the spectra of **6** and **10** are similar to those of **1** or **2**. The intensity of the 265 nm band decreases for the shorter sequences, resulting in an apparent red-shift in the negative band position from 250 nm for the longer sequences to 260 nm for **3**. Above 300 nm, **3**−**6** display bissignate CD spectra with maxima near 340 nm and minima near 300 nm or visa versa. The CD spectra of conjugates **7**, **11**, and **12** are shown in Figure 4d. The presence of a single G−C base pair is seen to result in pronounced changes in the 225−275 nm region of the CD spectrum. Both **7** and **11** have strong negative bands near 340 nm and weak positive bands near 300 nm, similar to those of **5** and **9**. However, **12** shows only a single weak band, similar to that of **2**, above 300 nm.

Transient Absorption Spectra. The picosecond time-resolved absorption spectra of **1** and **2** have previously been reported.[3,11] The spectrum of **1** consists of a relatively broad band with a band maximum at 570 nm and a transient decay

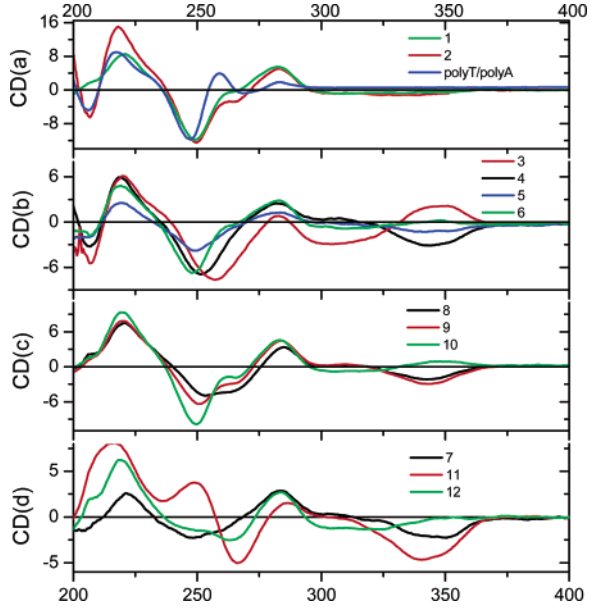

Figure 4. Circular dichroism spectra of conjugates **1**−**12** (ca. 10^{-6} M) and poly(A)−poly(T).

time identical to the fluorescence decay time (τ_S, Table 2). This transient is assigned to the singlet state of the **Sa** linker which is not quenched by T:A base pairs. The transient spectrum of **2** consists of a narrower band with a maximum at 530 nm. This transient is assigned to the cation radical of the **Sd** linker which is formed during the exciting laser pulse (<0.5 ps) via electron transfer to the neighboring T:A base pair. The radical ion pair state decays via charge recombination with a decay time of 32 ps (τ_I Table 2).

Normalized time-resolved transient absorption spectra of conjugate **3** are shown in Figure 5a. The spectrum observed 5 ps after 360 nm excitation (absorbed predominantly by **Sa**) is assigned to $^1\mathbf{Sa}^*$ (575 nm maximum and 625 nm shoulder). At longer delay times, the 625 nm shoulder disappears and maxima are observed at 525 and 575 nm, assigned to $\mathbf{Sd}^{+\bullet}$ and $\mathbf{Sa}^{-\bullet}$, respectively. Similar spectra are observed for conjugate **4** (Figure 5b); however the rise of the 525 component is less pronounced after 500 ps than is the case for **3**. The time-resolved spectra of **7** and **11** are similar to those of **3**. The 525 maximum is poorly resolved (**4** and **8**) or absent (**5**, **6**, **10**, and **12**) for the other conjugates.

Single wavelength picosecond and nanosecond transient decay profiles for conjugate **3** monitored at 575 and 525 nm are shown in Figure 6. The 575 nm decay is best fit as triexponential, the short-lived component (5−10 ps) being assigned to relaxation of $^1\mathbf{Sa}^*$, the medium component, to charge separation, and the long-lived component, to charge recombination. The 525 nm decay of **3** displays both rising and falling components with time constants similar to those for the two 575 nm components and assigned to the formation and decay, respectively, of $\mathbf{Sd}^{+\bullet}$.[11] Decay times and amplitudes for the 575 and 525 nm decays assigned to decay of $^1\mathbf{Sa}^*$ and $\mathbf{Sa}^{-\bullet}$, for conjugates **3**−**12**, are reported in Table 2.

Discussion

Conjugate Structure. The design of the **Sa**−**Sd** conjugates **3**−**12** is based on our finding that **Sa**- and **Sd**-linked bis-(oligonucleotide) conjugates such as **1** and **2** form exceptionally

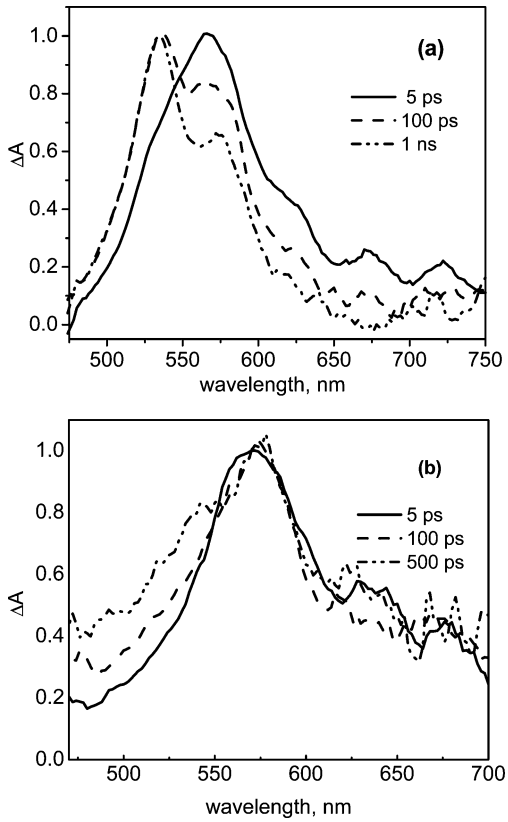

Figure 5. Normalized transient absorption spectra of **3** (a) and **4** (b) obtained at the indicated delay times following 360 nm excitation with a 0.13 ps laser pulse.

stable synthetic DNA hairpins.[9,10] The crystal structure of an **Sd**-linked hairpin possessing six base pairs displays a classic B-DNA base-paired stem with a compact loop in which the **Sd** linker is π-stacked with the adjacent base pair.[12] We have recently reported that addition of a second **Sa** to the 3′ end of an **Sa**-linked hairpin (e.g., **13**, Chart 2) results in further stabilization of the hairpin conjugate by ca. 2.3 kcal/mol.[13] We have referred to such molecules as "end-capped" hairpins, based on their similarity to the end-capped duplexes studied by Kool and co-workers.[14] Investigation of the distance-dependent EC/CD spectra of the end-capped hairpins revealed the stepwise evolution of the helical B-DNA structure of the A-tracts separating the two **Sa** chromophores.[13]

The **Sa**−**Sd** conjugates **3**−**12** were prepared with the intent of positioning of electron acceptor and electron donor chromophores at opposite ends of a π-stacked array of DNA base pairs. We previously proposed that conjugates **3**−**6** adopt mini-triplex structures in which the **Sd** linker forms a second hairpin connecting Hoogsteen-bound canonical TA−T triplets.[8] The tentative assignment of triplex structures was based on the melting profiles of **3**−**6** which display hyperchromism below the melting transition which becomes more pronounced as the length of the base sequences is increased (Figure 2a). This might

Chart 2

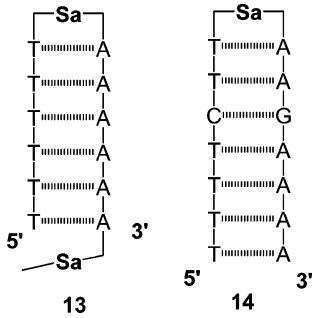

be attributed either to the melting of the triplex Hoogsteen strand or simply to melting of a poly(T) single strand. Intramolecular triplex formation has been achieved using both natural and synthetic hexakis(ethylene glycol) and 1,8-octanediol linkers.[15] However these triplex structures possess both TA−T and CG−C^+ triplets. To our knowledge, no intramolecular triplex possessing only TA−T triplets has been reported. The shortest reported intermolecular poly(TA−T) triplex possesses 19 triplets.[16]

Conjugates **8**−**10** cannot form triplex structures due to the inability of the single 5′-C to form a stable Hoogsteen triplet. The addition of the 5′-C incorporates the **Sd** linker into a bis-(oligonucleotide) sequence, as is the case for **3**−**7**. The structures of conjugates **8**−**10** are readily assigned as end-capped hairpins on the basis of comparison of their melting profiles (Figure 2b) and 200−300 nm CD spectra (Figure 4c) with those of **Sa**−**Sa** systems such as **13** (Chart 2).[13] The 200−300 nm region of the CD spectrum is dominated by base-pair exciton coupling.[17] The melting profile for **10** is very sharp, with little hyperchromism below the melting transition. The CD spectra for **8**−**10** show the development of spectra characteristic of poly(A)−poly(T) duplexes with increasing numbers of A−T base pairs, similar to that for **Sa**−**Sa** systems with three, four, and six base pairs.[13] Poly(A)−poly(T) duplex segments are known to form relatively rigid and linear structures known as A-tracts.[18] An interesting feature in the CD spectra of **8**−**10** is the evolution the 265 nm shoulder, which becomes a distinct maximum in the spectrum of poly(A)−poly(T) (Figure 4a). The other maxima and minima are well-defined with as few as two or three A−T base pairs.

The similarity of the CD spectra of **6** and **10** (Figure 4) suggests that **6** exists predominantly as an end-capped hairpin with an unbound poly(T) single strand region. Particularly telling is the presence of a strong positive 220 nm band for **6**, which is present in the CD spectrum of duplex poly(A)−poly(T) but not the corresponding triplex.[19] Additional evidence for an end-capped hairpin structures for **3**−**7** is provided by the absence of nonexchangeable imino N−H protons for the 3′-poly(T) sequence in the 600 Hz spectrum of **6** and by the long-wavelength CD spectra and electron-transfer dynamics of **3**−**7** (vide infra).

(12) (a) Lewis, F. D.; Liu, X.; Wu, Y.; Miller, S. E.; Wasielewski, M. R.; Letsinger, R. L.; Sanishvili, R.; Joachimiak, A.; Tereshko, V.; Egli, M. *J. Am. Chem. Soc.* **1999**, *121*, 9905−9906. (b) Egli, M.; Tereshko, V.; Mushudov, G. N.; Sanishvili, R.; Liu, X.; Lewis, F. D. *J. Am. Chem. Soc.* **2003**, *125*, 10842−10849.
(13) Lewis, F. D.; Liu, X.; Wu, Y.; Zuo, X. *J. Am. Chem. Soc.* **2003**, *125*, 12729−12731.
(14) Kool, E. T.; Morales, J. C.; Guckian, K. M. *Angew. Chem., Int. Ed.* **2000**, *39*, 990−1009.
(15) (a) Tarköy, M.; Phillips, A. K.; Schultze, P.; Feigon, J. *Biochemistry* **1998**, *37*, 5810−5819. (b) Bartley, J. P.; Brown, T.; Lane, A. N. *Biochemistry* **1997**, *36*, 14502−14511.
(16) Roberts, R. W.; Crothers, D. M. *Proc. Natl. Acad. Sci. U.S.A.* **1996**, *93*, 4320−4325.
(17) Johnson, W. C. In *Circular Dichroism, Principles and Applications*; Berova, N., Nakanishi, K., Woody, R. W., Eds.; Wiley-VCH: New York, 2000; pp 741−768.
(18) Dickerson, R. E.; Goodsell, D. S.; Niedel, S. *Proc. Natl. Acad. Sci. U.S.A.* **1994**, *91*, 3579−3583.
(19) Howard, F. B.; Miles, H. T.; Ross, P. D. *Biochemistry* **1995**, *34*, 7135−7144.

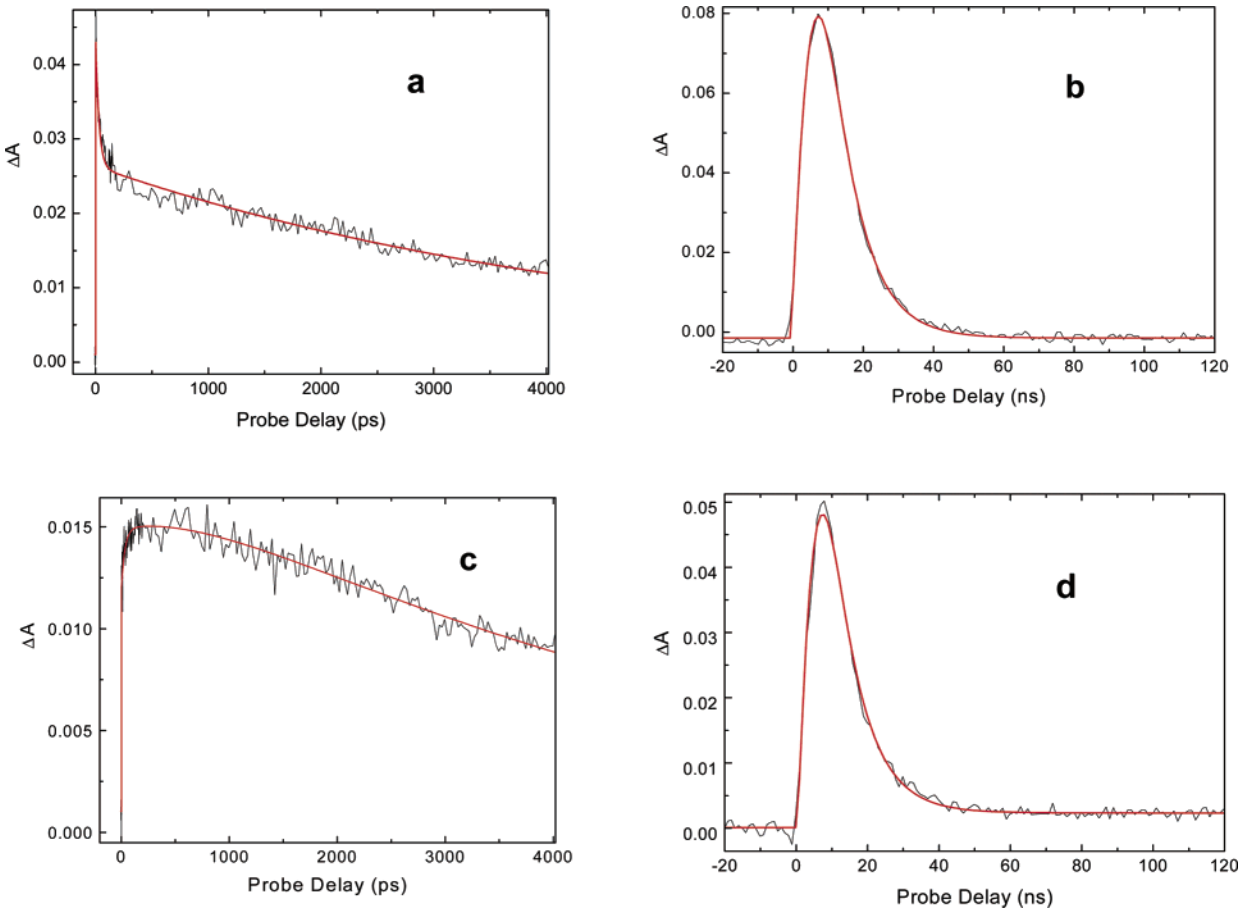

Figure 6. Transient decays for conjugate **3** on picosecond time scale at (a) 570 nm and (c) 525 nm and on nanosecond time scale at (b) 575 nm and (d) 530 nm.

Conjugates **11** and **12** are rendered in Chart 1 as nicked mini-dumbbell structures. Nicked dumbbells with natural nucleobase linkers have been prepared for the investigation of chemical and enzymatic ligation.[20] Conjugates **11** and **12** have much shorter base-pair regions than do previously investigated nicked dumbbells. The melting transitions of **11** and **12** are broader than those of **9** and **10**, respectively (Figure 2b), which have the same number of base pairs. The values of T_M are dependent upon the number of **Sd**-linked base pairs and are similar to the values expected for **Sd**-linked hairpins, respectively, with two and four base pairs, including one G−C base pair.[10] Thus the hyperchromicity observed below the melting transition may arise from premelting of the AA−**Sa**−TT mini-hairpin. The CD spectra of conjugates **7**, **11**, and **12** (Figure 4d) differ from those of the other conjugates in the region between 225 and 275 nm, presumably due to disruption of the A-tract geometry and base-pair exciton coupling by the presence of a G−C base pair. The similarity in the stilbene EC/CD spectra and electron-transfer dynamics for **11** and **7** (vide infra) provides the best evidence for a nicked dumbbell structure for **11**.

Exciton Coupled Circular Dichroism. The CD spectra of conjugates **1** and **2** display a single weak band at long wavelengths (>300 nm), assigned to the induced circular dichroism of the stilbene chromophore.[10] The appearance of these bands is similar to those achiral intercalators in which the long axis of the intercalator is approximately positioned parallel to the long axis of the adjacent base pairs.[21] The CD spectra of **3**−**11** are more complex, displaying two bands at long wavelengths with either a plus−minus (conjugates with 2 or 6 base pairs) or a minus−plus pattern (conjugates with 3 or 4 base pairs). These bands are attributed to exciton coupling (EC) between the **Sa** and **Sd** chromophores.[22] The appearance of the EC/CD spectra of **3**−**6** and **8**−**10** is similar to that of the corresponding end-capped hairpins having two **Sa** chromophores separated by the same number of A−T base pairs (e.g., **13**, Chart 2).[13] The greater rotational strength of the longer wavelength bands in Figure 4 is a consequence of the nonsymmetrical nature of the stilbene absorption bands (Figure 1) which have greater intensity at longer wavelength.

The weak exciton coupling (Davydov splitting), V_{da}, between two stilbenes separated by two or more base pairs can be described by eq 1a, where R_{da} is the distance vector between the two stilbenes and μ_d and μ_a are their electronic transition dipole moments. Since the distance vector is approximately perpendicular to the stilbene dipole moment vectors, eq 1a can be simplified as eq 1b.

$$V_{da} \approx (\vec{\mu}_d \cdot \vec{\mu}_a)R_{da}^{-3} - 3(\vec{\mu}_d \cdot \vec{\mu}_{da})(\vec{\mu}_{da} \cdot \vec{\mu}_a)R_{da}^{-5} \quad (1a)$$

$$V_{da} \approx (\vec{\mu}_d \cdot \vec{\mu}_a)R_{da}^{-3} \quad (1b)$$

(20) Ashley, G. W.; Kushlan, D. M. *Biochemistry* **1991**, *30*, 2927−2933.
(21) Ardhammar, M.; Nordén, B.; Kurucsev In *Circular Dichroism, Principles and Applications*; Berova, N., Nakanishi, K., Woody, R. W., Eds.; Wiley-VCH: New York, 2000; pp 741−768.
(22) Berova, N.; Nakanishi, K. In *Circular Dichroism*; Berova, N., Nakanishi, K., Woody, R. W., Eds.; Wiley-VCH: New York, 2000.

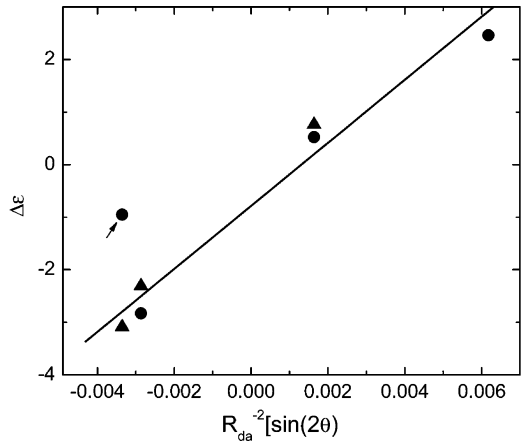

Figure 7. Intensity of the 340 nm CD band vs R_{da}^{-2} sin(2θ) for conjugates **3**−**6** (●) and 8−10 (▲). The line is the least-squares fit to the data (omitting the indicated data point).

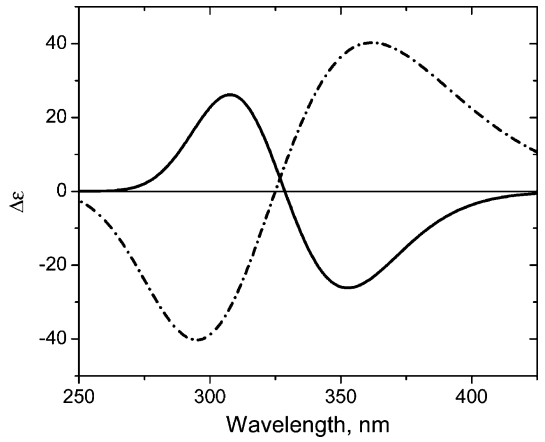

Figure 8. Simulated CD spectra for conjugate **5** obtained using a duplex geometry with four base pairs (solid line) or a triplex geometry with four TA−T triplets (broken line).

The sign and amplitude, $\Delta\epsilon$, of the EC/CD spectrum can be described by eq 2a,

$$\Delta\epsilon \approx \pm\frac{\pi}{2\lambda}\vec{R}_{da} \cdot \vec{\mu}_d \times \vec{\mu}_a \cdot V_{da} \qquad (2a)$$

$$\Delta\epsilon \approx \pm\frac{\pi}{4\lambda}\mu_a\mu_d R_{da}^{-2}\sin(2\theta) \qquad (2b)$$

which can be simplified (because the distance vector is perpendicular to the stilbene transition dipole vectors) to provide eq 2b, where θ is the angle between the two stilbene transition dipoles.[23] Increasing the number of base pairs separating the chromophores changes the sign and intensity of the CD spectrum as a consequence of the changes in both the distance and dihedral angle between the chromophores. According to eq 2b, the rotational strength should display an R_{da}^{-2} dependence and have maximum intensity when the dihedral angle between the chromophores is approximately 45° but zero intensity when they are parallel or perpendicular.

A plot of $\Delta\epsilon$ vs R_{da}^{-2}sin(2θ) obtained using the experimental data for conjugates **3**−**6** and **8**−**10**, assuming an average π-stacking distance of 3.4 Å, a B-DNA geometry, and a dihedral angle of 17° between both stilbenes and the adjacent base pair is shown in Figure 7. This geometry is the same as that obtained from our analysis of the EC/CD spectra of **Sa**−**Sa** end-capped hairpins.[13] A good linear fit to the data from Figure 4 is obtained with $R = 0.98$, omitting the data for conjugate **4**. To our knowledge, Figure 7 provides the first example of a quantitative correlation of rotational strength with the distance and dihedral angle separating two chromophores.

The observation of similar EC/CD spectra for conjugates **3**−**6**, **8**−**10**, and the **Sa**−**Sa** end-capped hairpins (Chart 2) requires that they have similar structures. This provides additional evidence for the formation of end-capped hairpin structures rather than intramolecular triplex structures by **3**−**6**. We have reported that the calculated CD spectra for the **Sa**−**Sa** end-capped hairpins agree with the experimental spectra only if an end-capped geometry with similar vector angles between the stilbenes at both ends of the base-paired duplex and the adjacent base pairs is assumed.[13] The simulated EC/CD spectra for **5** using the TA−T triplex geometry reported by Liu et al.[24] is shown in Figure 8 along with the simulated CD spectrum for an end-capped hairpin with four T−A base pairs. The simulated end-capped hairpin spectrum is similar to the experimental spectra of **5** and **7**, whereas the simulated triplex spectrum is of opposite sign.

Scheme 1

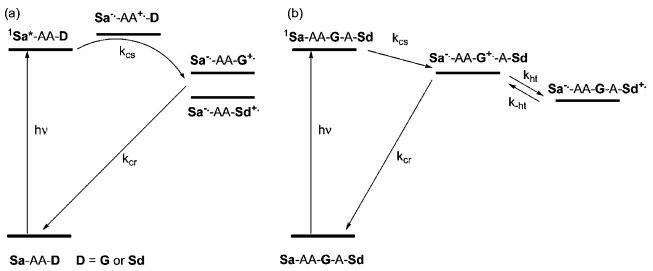

The EC/CD spectra of conjugates **5**, **7**, **9**, and **11** all display a relative strong negative band near 340 nm and a weak positive band near 300 nm. The uniform appearance of the EC/CD spectra for these conjugates requires that the distance and dihedral angles between the stilbenes be similar for end-capped hairpins and the nicked dumbbell **11**. This is consistent with the reported crystal structure of a nicked ternary DNA system in which the two T bases on either side of the nick have normal base stacking geometries.[25] The similarity of the long-wavelength CD spectra of **5**, **7**, **9**, and **11** further suggests that the appearance of the EC/CD spectrum is dependent upon the duplex structure but not the specific base sequence. The absence of apparent coupling between the stilbenes and bases no doubt reflects the large energy gap between their transitions, which should result in very weak coupling.

Dynamics of Charge Separation and Charge Recombination. We have previously investigated the distance-dependent dynamics of charge separation and charge recombination in **Sa**-linked hairpins containing a single G−C base pair (e.g., **14**, Chart 2).[1,3] As shown in Scheme 1a, electronic excitation of the **Sa** chromophore followed by selective oxidation of guanine yields the stilbene anion radical **Sa**$^{-\bullet}$ and the guanine cation

(23) (a) Cantor, C. R.; Schimmel, P. R. *Biophysical Chemistry*; W. H. Freeman: New York, 1980; Vol. 2. (b) Harada, N.; Nakanishi, K. *Circular dichroic spectroscopy: exciton coupling in organic stereochemistry*; University Science Books: Mill Valley, CA, 1983.

(24) Liu, K.; Sasisekharan, V.; Miles, H. T.; Raghunathan, G. *Biopolymers* **1996**, *39*, 573−589.

(25) Aymami, J.; Coll, M.; van der Marel, G. A.; van Boom, J. H.; Wang, A. H.; Rich, A. *Proc. Natl. Acad. Sci. U.S.A.* **1990**, *87*, 2526−2530.

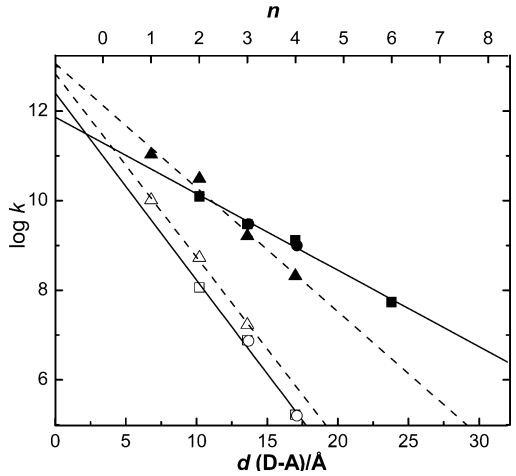

Figure 9. Distance dependence of the rate constants obtained from transient absorption data for charge separation (filled symbols) and charge recombination (open symbols) from conjugates **3**−**6** (square), **8**−**9** (circle), and **Sa**−**G** hairpin conjugates (triangle). *n* is the number of AT base pairs separating the donor and acceptor, and *d* is the distance calculated assuming a 3.4 Å base stacking distance.

radical ($\mathbf{G}^{+}\cdot$). The free energy for a photoinduced charge separation process (k_{cs}) can be estimated using Weller's equation (eq 3),

$$\Delta G_{cs} = -(E_S + E_{rdn}) + E_{ox} \quad (3)$$

where E_S is the singlet energy of the excited chromophore and E_{rdn} and E_{ox} are the redox potentials of the acceptor and donor.[26] A value of $\Delta G \approx -0.22$ eV is calculated from the **Sa** singlet energy (3.35 eV) and reduction potential (−1.91 V vs SCE in DMF solution) and the **G** oxidation potential (1.22 V vs SCE in acetonitrile).[3,27] The radical ion pair returns to the ground state via charge recombination (k_{cr}). The rate constants for charge separation and charge recombination are distance-dependent, decreasing as the number of A−T base pairs separating the **Sa** linker and G−C base pair increases, as expected for a superexchange electron-transfer process. The distance dependence can be described by eq 4,

$$k_{et} = k_o \exp(-\beta R_{da}) \quad (4)$$

where R_{da} is the distance between the donor and acceptor stilbenes and β is a constant which is dependent upon the donor−bridge−acceptor energetics of the system. Plots of the previously reported distance dependence of $\log(k_{cs})$ and $\log(k_{cr})$ for the **Sa**−**G** hairpins are shown in Figure 9.

In conjugates **3**−**6** and **8**−**10**, **Sa** serves as the electron acceptor, and **Sd**, as the electron donor. The value of $\Delta G = -0.52$ V, estimated from the **Sd** oxidation potential (0.92 V),[11] is more exergonic than that for the oxidation of **G** (Scheme 1a). However, the energy gap between the initial state and poly(A) bridging states are identical. Thus the tunneling energy gap and hence the magnitude of β would be expected to be similar for systems **G** or **Sd** as the donor.[28]

The normalized transient absorption spectra of conjugates **3** and **4** (Figure 5) obtained 5 ps after excitation at 360 nm display a band with a maximum at 575 nm and a shoulder at 625 nm, assigned to ^{1}**Sa***. Any ^{1}**Sd*** formed upon 360 nm excitation would be quenched by the adjacent A−T base pair in <1 ps.[11] The initial fast decay of the 575 nm absorption is accompanied by the rise of the 525 nm band attributed to formation of $\mathbf{Sd}^{+}$. The residual 575 nm band is assigned to a combination of $\mathbf{Sa}^{-\bullet}$ and unquenched ^{1}**Sa***. In the case of **3**, the decay of ^{1}**Sa*** is largely complete within 1000 ps, whereas, in the case of **4**, it is approximately half-quenched after 500 ps. The transient spectra for **8** are similar in appearance to those of **4**. The transient spectra of conjugates **5** and **9** display 525 nm shoulders 500 ps after the exciting laser pulse, indicative of slower formation of $\mathbf{Sd}^{+\bullet}$. Conjugates **6** and **10** display no change in band shape 500 ps after laser excitation.

The 575 and 525 nm single-wavelength decay components assigned to decay of the singlet state (τ_S) and of the radical ions (τ_I) are reported in Table 2. The rate constant for charge separation can be calculated from the decrease in the singlet lifetime for the **Sa**−**Sd** conjugates compared to the **Sa**-linked hairpin **1** ($k_{cs} = \tau_S^{-1} - 5 \times 10^8$ s^{-1}), whereas the rate constant for charge recombination is obtained directly from the decay time of the radical ions ($k_{cr} = \tau_I^{-1}$s^{-1}). Values of k_{cs} and k_{cr} are summarized in Table 2. The values of k_{cr} are considered to be more reliable, since there is a single long-lived nanosecond decay component for **3**−**5**. The value of k_{cs} for **6** is based on a small difference in two singlet decay times which are too short for nanosecond measurement but rather long for picosecond measurement with our instrumentation. Plots of $\log(k_{cr})$ and $\log(k_{cs})$ vs the donor−acceptor distance (R_{da}) for conjugates **3**−**6** and **8**−**9** are shown in Figure 9 along with data for the **Sa**−**G** hairpins. The value of β obtained for charge separation in the **Sa**−**Sd** conjugates is smaller than that for **Sa**−**G** hairpin charge separation ($\beta_{cs} = 0.40 \pm 0.1$ Å^{-1} vs 0.65 ± 0.15 Å^{-1}), whereas the values of β for charge recombination are similar for the **Sa**−**Sd** and **Sa**−**G** systems ($\beta_{cr} = 1.0 \pm 0.1$ Å^{-1} vs 0.94 ± 0.1 Å^{-1}). Whether the difference in values for charge separation reflects differences in donor−bridge−acceptor geometry or energetics or is simply a consequence of limited data remains uncertain.

Conjugates **7** and **11** differ from **5** and **9**, respectively, by the substitution of a G−C base pair for the T−A base pair located at the third base-pair position relative to the **Sa** acceptor. Our earlier studies of **Sa**−**G** hairpin systems provided values of $\tau_S = 120$ ps and $\tau_I = 3.8$ ns for the hairpin **14** (Chart 2) in which the G−C base pair located at the third base pair.[3] The values of τ_S for **7** and **11** are similar to that for the **Sa**−**G** hairpin and significantly shorter than the values for **5** and **9** (Table 2). Thus we conclude that **G**, rather than **Sd**, is the primary electron donor in the charge separation process for conjugates **7** and **11**. Comparison of the τ_S values for **12** vs **10** indicates that **G** also serves as the primary donor in **12**.

The values of τ_I for **7** and **11** are, however, much longer than those for the **Sa**−**G** hairpin **14** and are similar to those for the **Sa**−**Sd** end-capped hairpins **5** and **9**. This is consistent with the occurrence of hole transport from **G** to **Sd** in **7** and **11**, creating a long-lived charge-separated state (Scheme 1b). The values of τ_I for **7** and **11** are also similar to those for **Sa**-linked hairpins with an **Sa**−**AAGAZA** (Z = deazaguanine) hole transport sequence ($\tau_I = 6000$ ns).[29] The oxidation potentials of **Sd** and **Z** are similar, and thus the energetics of charge

(26) Weller, A. *Z. Phys. Chem., Neue Folge* **1982**, *133*, 93−98.
(27) Seidel, C. A. M.; Schulz, A.; Sauer, M. H. M. *J. Phys. Chem.* **1996**, *100*, 5541−5553.
(28) Lewis, F. D.; Liu, J.; Weigel, W.; Rettig, W.; Kurnikov, I. V.; Beratan, D. N. *Proc. Natl. Acad. Sci. U.S.A.* **2002**, *99*, 12536−12541.

recombination should be the same for both systems. In the case of **7**, a shorter-lived decay component is also observed (Table 2). This might arise from competitive hole transport and charge recombination in the primary $\mathbf{Sa}^{-\bullet}-\mathbf{G}^{+\bullet}$ charge separated state.[4] In the case of **12**, no long-lived charge separated state is observed, indicative of the failure of hole transport across an $(A-T)_4$ sequence to compete with charge recombination in the primary charge separated state. This is consistent with the distance dependence for hole transport observed in our earlier studies.[4]

Comparison of Exciton Coupling and Electron Transfer. According to eq 2a, the rotational strength of the EC/CD bands should display an $R^{-2}\sin(2\theta)$ dependence on the distance and vector angle between the **Sa** and **Sd** transition dipoles. The decrease in intensity (Figure 7) and sign changes for the EC/CD spectra of **3**−**6** and **8**−**10** (Figure 4b,c) are consistent with this expectation. The similar spectra for **4** and **7** indicate that the EC/CD spectra are not sensitive to the specific base pairs separating the chromophores. The base pairs, in essence, serve as a helical scaffold upon which the stilbene chromophores are positioned but do not mediate the exciton coupling process.[13]

According to eq. 4, the rate constants for charge separation and charge recombination (Scheme 1a) should display an exponential dependence on R_{da}, in agreement with the experimental data (Figure 9). According to tunneling theory, the rate constant can be described as the product of H_{DA}, the electronic coupling between the donor and acceptor, and FC, the Frank−Condon factor (eq 5).[28]

$$k_{et} = \frac{2\pi}{\hbar}|H_{DA}|^2 \mathrm{FC} \tag{5}$$

For electron transfer through a vacuum, H_{DA} would be expected to be dependent upon the angle between the donor and acceptor chromophores as well the distance between them. However, for bridge-mediated superexchange, electron transfer is promoted by the π-stacking interaction of the intervening base pairs. The absence of angle dependence in the experimental data can be explained in terms of the McConnell model, according to which the distance dependence, β (eq 4), can be described by eq 6,

$$\beta = (2/R_o)\ln|\Delta E/t_{mn}| \tag{6}$$

where ΔE is the energy gap between the donor (or acceptor) and base-pair bridge orbitals and t_{mn} is the interaction element between nearest neighbor bridging states.[30] Since the angle between base pairs is approximately constant, the involvement of the base-pair eigenstates may serve to eliminate the angular dependence of k_{et}, which would be expected if the base pairs served solely as a helical scaffold positioning the donor and acceptor at a fixed geometry. The base-pair sequence is also of crucial importance for the electron-transfer process, as evidenced by the marked decrease in τ_S observed for conjugate **7** vs **5** (Table 2). Introduction of a G−C base pair changes the mechanism for charge separation from a single step tunneling process for **5** (Scheme 1a) to a multistep hole transport process for **7** (Scheme 1b).

Concluding Remarks. The structure and properties of oligonucleotide conjugates containing both electron acceptor and electron donor stilbene linkers have been investigated. Conjugates **3**−**10**, which possess a Watson−Crick hairpin-forming sequence and an additional 3′-poly(T) or 5′-C, form end-capped hairpin structures similar to those we have reported recently for **Sa**−**Sa** conjugates such as **13** (Chart 2). Thus the 3′-poly(T) sequence of **3**−**7** evidently does not form a mini-triplex by Hoogsteen binding in the major groove of the Watson−Crick hairpin. Conjugates **11** and **12** form nicked dumbbell structures with geometries similar to those of the end-capped hairpins **3**−**10**. Circular dichroism spectroscopy provides evidence for both the B-form structure of the A-tracts in conjugates **3**−**6** and **8**−**10** and for the relative positions of the stilbene chromophores at the opposite ends of the end-capped hairpin and nicked dumbbell structures. The helical nature of the short duplex regions in **3**−**12** is clearly evidenced by the dependence of both the sign and the intensity of the stilbene EC/CD spectra on the number of base pairs separating the two stilbenes.

Transient absorption spectroscopy of conjugates **3** and **4** on the picosecond and nanosecond time scales provides the first direct evidence for the oxidation of an electron donor separated from an excited electron acceptor by a variable number of base pairs. For larger donor−acceptor separations, the occurrence of charge separation is inferred from the dynamics of the nanosecond decay of $\mathbf{Sa}^{-\bullet}$, as previously reported for **Sa**−**G** hairpin systems. In the case of conjugates **7** and **11**, which possess **Sa**−AAGA−**Sd** hole transport sequences, the accelerated formation of long-lived transients is consistent with the occurrence of hole transport from the guanine primary donor to the **Sd** secondary donor. The extraordinary thermodynamic stability of the **Sa**−**Sd** end-capped hairpins and the occurrence of photoinduced electron transfer in these systems suggests that end-capped hairpins may be suitable for studies of the efficiency and dynamics of multistep electron transfer across substantially longer base-pair sequences.

The observation of both EC/CD and PET for these conjugates permits, for the first time, a comparison of the distance dependence of these processes. The two processes display R_{da}^{-2} and $\exp(R_{da})$ dependence, respectively. In addition, the EC/CD process displays a marked dependence upon the vector angle relating the donor and acceptor transition dipoles, whereas the PET process displays no perceptible angular dependence. This notable difference is attributed to the involvement of the base-pair virtual states in the PET process but not in the EC/CD process. The absence of coupling between the stilbene and base-pair chromophores in the ground state is a consequence of the large energy gap between the stilbene and nucleobase electronic transitions.

Experimental Section

General Methods. Methods for obtaining UV absorption, fluorescence, and circular dichroism spectra and for the measurement of fluorescence quantum yields have been previously described.[3] Fluorescence spectra were obtained for solutions of ca. 2×10^{-6} M conjugate in aqueous phosphate buffer (10 mM, pH 7.2) containing 0.1 M NaCl and were deoxygenated by purging with dry nitrogen. Transient absorption spectra were recorded using either a femtosecond or nanosecond pulsed laser-based system.[31]

(29) Lewis, F. D.; Liu, J.; Liu, X.; Zuo, X.; Hayes, R. T.; Wasielewski, M. R. *Angew. Chem., Int. Ed.* **2002**, *41*, 1026−1028.
(30) McConnell, H. M. *J. Chem. Phys.* **1961**, *35*, 508−515.
(31) Lewis, F. D.; Liu, X.; Miller, S. E.; Hayes, R. T.; Wasielewski, M. R. *J. Am. Chem. Soc.* **2002**, *124*, 14020−14026.

Materials. The bis(3-hydroxypropyl)amide of stilbene-4,4′-dicarboxylic acid[9] and the bis(2-hydroxyethyl)stilbene 4,4′-diether[10] were prepared and converted to their mono-DMT derivatives by reaction with 4,4′-dimethoxytrityl chloride. The mono-DMT derivatives were reacted with 2-cyanoethyl diisopropylchlorophosphoramidite to afford the monoprotected, monoactivated diols. The preparation, purification, and characterization of the oligonucleotide conjugates **1**−**12** followed the method of Letsinger and Wu[9] as implemented by Lewis et al..[10] The 3′−3′ linkages between the Watson−Crick T:A hairpin sequence and the polyT strand attached to the **Sd** linker in conjugates **3**−**7** were accomplished by 5′ solid-phase oligonucleotide synthesis. Molecular weights of selected conjugates were determined by electrospray ionization mass spectroscopy using a Micromass Quattro II Atomospheric Pressure Ionizaton system. Conjugates were purified using a Nensorb 20 Nucleic Acid Purification Cartridge prior to direct loop injection.

Acknowledgment. This research is supported by grants from the Division of Chemical Sciences, Office of Basic Energy Sciences, U.S. Department of Energy under Contract DE-FG02-96ER14604 (F.D.L.) and DE-FG-02-99ER14999 (M.R.W.). We thank Robert L. Letsinger for stimulating our interest in hairpin-forming DNA conjugates and Alexander Burin (Tulane University) for suggestions pertaining to the angular dependence of electron transfer.

JA048664M